HHS Public Access

Author manuscript

Nat Med. Author manuscript; available in PMC 2016 April 01.

Published in final edited form as:

Nat Med. 2015 October ; 21(10): 1154–1162. doi:10.1038/nm.3951.

Critical Role of Acetylation in Tau-Mediated Neurodegeneration and Cognitive Deficits

Sang-Won Min[1,2,#], **Xu Chen**[1,2,#], **Tara E Tracy**[1,2], **Yaqiao Li**[1], **Yungui Zhou**[1], **Chao Wang**[1,2], **Kotaro Shirakawa**[3], **S. Sakura Minami**[1,2], **Erwin Defensor**[4], **Sue Ann Mok**[5], **Peter Dongmin Sohn**[1,6], **Birgit Schilling**[7], **Xin Cong**[7], **Lisa Ellerby**[7], **Bradford W. Gibson**[7], **Jeffrey Johnson**[8], **Nevan Krogan**[8], **Mehrdad Shamloo**[4], **Jason Gestwicki**[5], **Eliezer Masliah**[9], **Eric Verdin**[3,*], and **Li Gan**[1,2,6,*]

[1]Gladstone Institute of Neurological Disease, San Francisco, CA, USA

[2]Department of Neurology, University of California, San Francisco, CA, USA

[3]Gladstone Institute of Virology and Immunology, San Francisco, CA, USA

[4]Stanford Institute for Neuro-Innovation and Translational Neurosciences, Stanford University School of Medicine, Stanford, CA, USA

[5]Department of Pharmaceutical Chemistry, Institute for Neurodegenerative Disease, University of California, San Francisco, CA, USA

[6]Neuroscience Graduate Program, University of California, San Francisco, CA, USA

[7]Buck Institute for Research on Aging, Novato, CA, USA

[8]Gladstone Institute of Cardiovascular Disease, San Francisco, CA, USA

[9]Department of Neuroscience, University of San Diego, San Diego, CA, USA

Abstract

Tauopathies, including frontotemporal dementia (FTD) and Alzheimer's disease (AD), are neurodegenerative diseases in which tau fibrils accumulate. Recent evidence supports soluble tau species as the major toxic species. How soluble tau accumulates and how it causes neurodegeneration remains unclear. Here we identified tau acetylation at K174 as an early change in AD brains and as a critical determinant in tau homeostasis and toxicity in mice. An acetyl-mimicking mutant (K174Q) slows down tau turnover and induces cognitive deficits *in vivo*. The acetyltransferase p300-induced tau acetylation is inhibited by a prescription drug salsalate/

*Correspondence: lgan@gladstone.ucsf.edu, eric.verdin@gladstone.ucsf.edu.
#Authors contribute equally

AUTHOR CONTRIBUTIONS

L.G., S-W.M. conceived the project, L.G., S-W.M., and X.C. designed experiments. S-W.M., X.C., T.T., P-D.S., S.A.M., C.W., K.S., S.S.M, E.D., B.S., X.C, J.J., Y.Z., Y.L., and E.M. performed experiments. L.E., B.W.G., M.S., J.G., N.K., and E.V. developed experimental tools or reagents. L.G., S-W.M, X.C wrote the manuscript.

COMPETING FINANCIAL INTERESTS

The authors declare no competing financial interests.

salicylate, which enhances tau turnover and reduces tau levels. In the PS19 transgenic mouse model of FTD, administering salsalate after disease onset inhibited p300 activity, lowered ac-K174 and total tau levels, rescued tau-induced memory deficits and prevented hippocampal atrophy. The tau-lowering and protective effects of salsalate/salicylate are diminished in neurons expressing K174Q tau. Targeting tau acetylation could be a new therapeutic strategy against human tauopathies.

Neurodegenerative tauopathies include brain disorders such as primary tauopathies (e.g., Pick's disease, frontotemporal dementia (FTD), progressive supranuclear palsy, and secondary tauopathies (e.g., Alzheimer's disease (AD))[1,2]. Tauopathies are characterized by neurofibrillary tangles (NFTs) of insoluble hyperphosphorylated tau fibrils. Although accumulation and distribution of NFTs have been used for diagnostic and staging purposes[3], recent evidence supports a key pathogenic role of soluble tau oligomers[4,5]. Increased levels of tau oligomers were detected in the frontal cortex of AD patients at early Braak stages[4,6]. In rodents, injection of recombinant tau oligomers, but not fibrils, impaired memory in wild-type mice[7]. In tauopathy mouse models, levels of tau oligomers correlate with memory loss at various ages[8]. Moreover, suppressing soluble tau improves cognitive function without reducing levels of insoluble NFTs in inducible tauopathy mouse models[9,10].

Both autophagic and proteasomal degradation pathways have been implicated in the tau clearance[11,12]. In AD brains, tau oligomers appear ubiquitinated and accumulate at synapses, where proteasome components are enriched[13]. Tau undergoes lysine acetylation[14,15], which modulates diverse biological processes including protein stability and protein-protein interactions[16]. Analyses of the soluble fraction of AD brain lysates showed that tau acetylation was enhanced in patients at early/moderate Braak stages, consistent with an early role of acetylation in modulating tau accumulation[14]. Acetylation, but not phosphorylation[17], regulates aggregation of recombinant tau *in vitro*[15,18]. Moreover, inhibiting the deacetylase sirtuin 1 (SIRT1) elevates tau acetylation, suppresses its polyubiquitination and slowed down its turnover in primary neurons[14]. However, it remains unclear which lysine residue(s) are aberrantly acetylated in AD brains, and whether they are key determinants in tau homeostasis *in vivo*.

Here, we identified K174 acetylation as an early critical pathological change to soluble tau in AD brains, using mass spectroscopy and a newly developed antibody specific for ac-tau. We further established a critical role of K174 in tau homeostasis and toxicity. Lastly, we tested the effects of a prescription drug salsalate, which inhibits p300-induced tau acetylation, on tau-mediated behavioral deficits and neurodegeneration in PS19 mice, an FTD model.

RESULTS

Tau Is Acetylated at Lysine-174 in Human AD Brains and Tauopathy Mice

To identify acetylated lysines on soluble tau, we used mild detergents to extract lysates from AD brains. Tau was immunoprecipitated from soluble AD lysates, followed by proteolytic digestion and analysis by high-performance liquid chromatography–electrospray tandem

mass spectrometry (HPLC-ESI-MS/MS). Lysine-174 on the native peptide IPA^{174}KacTPPAPK was identified to be acetylated (Fig. 1a) and this was confirmed with a synthetic peptide of the same sequence (Fig. 1b). To further characterize ac-K174 in AD brains, we generated a polyclonal rabbit antibody, AC312, with an antigen containing acetylated K163 and K174 (ac-K163 was included based on previous *in vitro* studies[14,15]). Incubating recombinant human tau (hTau, 2N4R, 441 amino acids) with the acetyltransferase p300 led to strong AC312-positive signals, which were non-detectable without p300 (Fig. 1c). A pan-tau antibody (Ab707)[14] detected comparable levels of tau with or without p300, suggesting AC312 is specific for acetylated-tau (ac-tau). To determine the specificity of AC312 for different tau ac-K residues, human embryonic kidney (HEK293) cells were transfected with WT or non-acetylatable mutant (KR) tau constructs with or without p300 co-expression. AC312 detected a strong p300-induced ac-tau signal in cells expressing WT tau or various KR mutants, except for K174R, indicating that AC312 is specific for ac-K174, although the peptide antigen contains ac-K163 (Fig. 1d).

We next assessed K174 acetylation in AD brains at different Braak stages (Supplementary Table 1), a well-established staging method that correlates cortical tau pathology progression with the worsening of clinical symptoms[3]. Human brain lysates were partially purified on a column with Tau5 antibody to reduce non-specific signal. Immunoblots with the Tau5 antibody showed similar levels of tau in each sample (Fig. 1e). In contrast, AC312 immunoreactivity was very weak or non-detectable in brain lysates at Braak stage 0, but was distinctively stronger in lysates at early (stages 1–2) and later (3–5) Braak stages (Fig. 1e,f). PHF-1-positive phosphorylated-tau (p-tau) signal was more readily detected at later (3–5) Braak stages. These findings suggest ac-K174 is among the early pathogenic alterations of tau in AD.

AC312 immunoreactivity was examined in PS19 mice, which express hTau with the P301S mutation under the mouse prion promoter, and develop cognitive and synaptic deficits that depend on hippocampal function[19]. The specificity of AC312 immunoreactivity was confirmed in non-transgenic and tau-knockout mice (Supplementary Fig. 1a). In 6-month-old PS19 mice when early pathological changes start to appear[19], pathological tau was detected with MC1, an antibody specific for a pathogenic conformation of tau that precedes formation of tangles[20,21]. AC312 and MC1 immunoreactivity exhibited remarkable co-localization along the mossy fiber of hippocampus (Fig. 1g–j, Supplementary Fig. 1b).

Acetyl-mimic K174Q Mutation Slows Tau Turnover *In Vitro* and Promotes Tau Accumulation *In Vivo*

We previously showed that augmenting tau acetylation via SIRT1 inhibition slowed tau degradation in cultured neurons *in vitro*[14]. To determine if ac-K174 is critical to slow tau turnover, we replaced lysine with glutamine (K174Q), which neutralizes the positive charge and mimics the acetylated state. Conversely, a K174R mutant was used to mimic deacetylated-tau. Both mutations are commonly used to assess the effects of acetylation[22–24]. To measure the hTau half-life, we infected rat primary neurons with lentiviral vectors expressing WT, K174Q, or K174R hTau, and quantified hTau levels in the presence of translation inhibitor cycloheximide (CHX). K174Q tau exhibited a longer half-

life than K174R or WT tau (Fig. 2a). Since polyubiquitination on K174 should be blocked by both K174Q and K174R mutants, acetylation of K174 *per se*, not blockage of polyubiquitation alone, seems to slow tau degradation.

We next determined the effects of ac-K174 on tau accumulation *in vivo* by injecting equal amount of adeno-associated virus type 1 (AAV1) vectors that express WT, K174Q, and K174R human tau (hTau) constructs into the hippocampus of 2–3 month old wildtype C57B6 mice. Tau overexpression is known to induce toxicity in hippocampus, which can be reliably targeted with AAV1 vectors. Direct comparisons were performed in two cohorts: K174Q vs WT and K174Q vs K174R. Immunostaining with an anti-hTau antibody, HT7, showed similar distributions of hTau throughout the hippocampus 10 days after injection (Fig. 2b,d). Similar levels of hTau transduction were maintained 3 months after injection, as determined by qRT-PCR (Fig. 2c,e). However, western blot analysis of hippocampal lysates revealed that monomeric K174Q tau levels were higher than those of WT tau (Fig. 2f,g-*left*) or K174R tau (Fig. 2h,i-*left*). Consistent with the effects of ac-tau on the half-life of tau *in vitro*, these results indicate that K174 acetylation *per se*, not the blockage of polyubiquitination alone, leads to monomeric tau accumulation *in vivo*. In addition, AAV-K174Q expression led to a marked increase in tau signal that migrates at ~140 kD, most likely dimeric tau (Fig. 2f,g-*right*; Supplementary Fig. 2). Interestingly, expressing K174R tau led to a similar increase of tau dimers as K174Q tau (Fig. 2h, i-*right*), supporting the importance of the K174 residue, but not acetylation *per se*, in tau aggregation. Indeed, recombinant K174Q and K174R tau showed a higher propensity for aggregation than WT tau *in vitro*, as indicated by the time-dependent increase of Thioflavin T–positive signals (Fig. 2j).

Acetylation of the KXGS motif suppresses tau phosphorylation at KIG(S)(Ser262/Ser356)[18]. K174Q expression in hippocampus did not significantly affect the levels of ac-K(IGS) (Supplementary Fig. 3) or p-KIG(S)(Ser262/Ser356) (Supplementary Fig. 4a,b). Levels of other p-tau species, including pThr231 (AT180+), pThr181 (AT270+) or pSer396 (PHF13+) were also not significantly affected by K174Q expression (Supplementary Fig. 4c–e). Interestingly, K174Q expression led to higher levels of AT8-positive p-tau (Ser202/Thr205) than WT or K174R tau in hippocampus (Supplementary Fig. 4f–i).

Hippocampal Expression of K174Q Tau Worsens Tau-Mediated Neurodegeneration and Behavioral Deficits

To determine how K174 acetylation affects toxicity of overexpressed hTau, we examined mouse hippocampal volumes three-month after injection of AAV1 vectors encoding WT, K174Q and K174R tau. As reported, AAV-induced expression of WT tau led to a loss of hippocampal volume[25]. Similar levels of K174Q tau induced worse hippocampal atrophy than WT (Fig. 3a) or K174R tau (Fig. 3b), suggesting that ac-K174 induces more severe neurodegeneration. To assess the functional outcome of elevated levels of ac-K174 in hippocampus, we used open field, small Y-maze, and Morris water maze (MWM) to measure hippocampal function. Hyperlocomotor activity in the open field is induced by hippocampal lesion[26]. Spontaneous alterations in the small Y-maze measure hippocampal-dependent spatial working memory, which was impaired in tauopathy mice expressing

human tau with P301S mutation[27]. MWM is one of most common tests for hippocampal-dependent spatial learning and memory.

In the open field, mice expressing K174Q exhibited significantly higher total activity than non-injected (NI) mice, while mice expressing comparable levels of WT or K174R tau behaved similarly as NI mice (Fig. 3c). Notably, the levels of K174Q tau monomers were positively correlated with total activity in the open field (Fig. 3d). In small Y-maze tests, hippocampal expression of K174Q, but not WT or K174R tau significantly reduced the percentage of spontaneous alternations (Fig. 3e), suggesting that ac-K174 tau impairs spatial working memory. In MWM tests, K174Q tau-expressing mice exhibited a slower learning curve than WT tau-expressing or NI mice in the first phase of spatial learning (Fig. 3f). K174Q tau-expressing mice also learned more slowly than K174R tau-expressing mice (Fig. 3h). After all groups were trained to criterion, we performed reversal training by moving the hidden platform to a new location. K174Q-, not WT tau- or K174R-expressing mice, located the new location more slowly than NI controls (Fig. 3f,h). These findings demonstrate that ac-K174 impairs spatial learning. In the probe trials that measure memory retention, K174Q tau-, not WT tau-expressing mice, crossed the target platform significantly fewer times than NI control mice, suggesting impaired memory retention induced by K174Q expression (Fig. 3g). The direct comparison between K174R and K174Q on memory retention was inconclusive since the NI control mice in this cohort showed no clear memory retention (Fig. 3i).

Inhibiting p300 Reduces Ac-TauK174 and Total Tau

The main acetyltransferases responsible for tau acetylation are p300 and its close homologue CBP[14,15]. To further examine the role of p300, we performed genetic deletion by infecting *p300*$^{F/F}$ primary mouse neurons with lenti-cre in culture (Fig. 4a). Deleting p300 lowered levels of total tau (t-tau), ac-K174, and p-tau (Ser202/Thr205) (Fig. 4b). Levels of ac-K174 or AT8-positive p-tau were also lowered relative to t-tau (Fig. 4c). We showed that pharmacological inhibition of p300 with C646 reduced levels of p-tau and ac-tau in primary neurons[14]. However, due to its poor brain permeability and pharmacokinetic (PK) properties (not shown), we tested other small molecules that inhibit p300, including salicylate, one of the non-steroid ant-inflammatory drugs (NSAIDs) (Shirakawa et al., unpublished). In HEK293 cells, salicylate reduces acetylation of H2AK5, a well-established substrate of p300, in a dose-dependent manner (Supplementary Fig. 5a). In rat primary neurons infected with a lentiviral vector encoding WT hTau (Lenti-WT), salicylate reduced levels of p300 (Fig. 4d, *left*). Levels of ac-K174 (Fig. 4d, *middle*) and AT8-positive p-tau (Fig. 4d, *right*), relative to t-tau, were also reduced by salicylate treatment. Consistent with the notion that ac-K174 inhibits tau degradation, reduction of ac-K174 with salicylate enhanced tau turnover in primary neurons (Supplementary Fig. 5b).

To examine the potential protective effects of p300 inhibition against tauopathy *in vivo*, we first sought to determine if p300 is aberrantly activated in the brains of PS19 mice. H3K18 acetylation has been used as a marker for p300/CBP activity since deleting p300 and its close homolog CBP leads to a complete loss of ac-H3K18[28–30]. Levels of ac-H3K18 were significantly higher in the brains of PS19 mice than those of age-matched controls (Fig. 4e).

To inhibit p300/CBP in the brain, we treated PS19 mice with salsalate (SSA), a prodrug of salicylate used in patients with rheumatoid arthritis. PK analysis showed that, upon absorption, SSA penetrates into the brain and gives rise to relatively stable salicylate levels over 8 h (Supplementary Fig. 6).

We investigated the effects of SSA treatment in PS19 mice after the onset of tau-mediated spatial memory deficits. Two independent cohorts were tested: one cohort of 8–9-month-old female PS19 mice and controls, and the other 7–8-month-old male PS19 mice and controls. The male and female cohorts were tested separately to avoid the confounding effects of sex hormones on the other gender in behavior tests. SSA (225 mg/kg) or vehicle was dosed by oral gavage. The length of the treatment for female cohort was 60 days and for the male cohort was 84 days. The dose of 225 mg/kg was well tolerated; no weight difference was observed in vehicle- and SSA-treated PS19 mice during treatment (not shown). Inhibition of brain p300 was examined by measuring acetylation levels of well-established substrates for p300/CBP[29–31], including ac-H3K18 (Fig. 4f), Ac-H2AK5 (Fig. 4g), or ac-H2BK12K15 (Fig. 4h), all of which were reduced significantly by SSA treatment. These results demonstrated clear target engagement of SSA at 225 mg/kg in the brain.

SSA treatment also reduced the levels of t-tau quantified with ELISA (Fig. 4i, *left*), while levels of tau mRNA were not affected (Fig. 4i, *right*). SSA did not affect acetylation or phosphorylation of the KXGS motif (Supplementary Fig. 7), consistent with a lack of effect induced by K174Q. Importantly, SSA induced a reduction in ac-K174 relative to t-tau, and a trend of reduction in AT8-positive p-tau, which did not reach significance when normalized to t-tau (Fig. 4j).

SSA Protects against Pathological Alterations and Spatial Memory Deficit in PS19 Mice

We next determined whether inhibiting K174 tau acetylation ameliorates tau-mediated pathological and behavioral deficits. PS19 mice exhibit hippocampal atrophy at advanced ages[32]. In the female cohort, at 8 months, hippocampal volume of PS19 and non-transgenic (NTG) mice was similar (Fig. 5a, b). At 10 months of age, vehicle-treated PS19 exhibited significant hippocampal atrophy compared with NTG controls; SSA completely prevented hippocampal atrophy, restoring volume similar to that of 8-month-old NTG or PS19 mice (Fig. 5a, b). Similarly, male SSA-treated PS19 mice also exhibited significantly less hippocampal atrophy at 10 months of age (Supplementary Fig. 8a, b). Prominent NFTs and dystrophic neuritis, positive for Gallyas silver staining, were detected throughout the forebrains in PS19 mice (Fig. 5c). SSA reduced the number of Gallyas silver-positive neurons and neurites in the cortex and hippocampus of PS19 mice, in both the female (Fig. 5c, d), and the male cohorts (Supplementary Fig. 8c, d).

To assess SSA's effects on tau-mediated spatial learning and memory deficits, we performed MWM or fixed-location dry maze, which is a modified Barnes maze that measures spatial learning and memory, but less physically demanding than MWM[33]. The male cohort was tested in MWM. The female PS19 mice were tested in the dry maze since they were slightly older and appeared physically weaker than those in the male cohort. Mice in the fixed-location dry maze learned to locate the escape hole using spatial cues in the spatial learning segment. We observed no significant difference in learning rates for locating the escape hole

among vehicle-treated NTG mice and vehicle- or SSA-treated PS19 mice (Fig. 5e). In the probe trial, while vehicle-treated NTG mice spent more time in the target quadrant than the non-target quadrant, vehicle-treated PS19 mice had no preference for the target quadrant, showing impaired memory retention and retrieval (Fig. 5f). SSA-treated PS19 mice spent more time in the target quadrant, showing improved spatial memory. Similarly, in the MWM, no spatial learning deficits were observed in the four groups (Fig. 5g). In the probe trial, vehicle-treated PS19 mice had no preference for the target quadrant (Fig. 5h). In contrast, SSA-treated PS19 mice showed similar preferences for the target quadrant as vehicle- or SSA-treated NTG groups, confirming SSA's protective effects against tau-mediated memory impairments.

Ac-K174 Inhibition as a Mediator of Salicylate/SSA's Tau-Lowering and Protective Effects

To investigate the mechanism underlying the tau-lowering effects of salicylate, primary rat neurons were infected with AAV-WT or AAV-K174Q hTau and treated with salicylate. Salicylate induced similar extent of p300 inhibition in neurons expressing WT (Fig. 6a,b) or K174Q hTau (Fig. 6d,e) as levels of p300 and mouse t-tau were similarly reduced. However, while salicylate lowered levels of human WT tau (Fig. 6c), it failed to reduce those of K174Q tau (Fig. 6f), suggesting that salicylate's tau-lowering effect requires inhibition of ac-K174 in primary neurons.

We next determined if SSA's beneficial effects involve inhibition of ac-K174 *in vivo*. Two-month after the injecting with AAV-K174Q, mice were treated with SSA daily as previously performed in PS19 mice. Ac-H2AK5 levels were reduced in the SSA-treated group, confirming inhibition of p300 by SSA (Fig. 6g). However, in contrast to the tau-lowering effects of SSA in PS19 mice, SSA treatment failed to reduce levels of t-tau in K174Q injected mice compared to vehicle treated controls (Fig. 6h). Levels of PHF1-postive p-tau relative to t-tau, or AT8-positive p-tau normalized by t-tau or GAPDH, were also not affected by SSA treatment (Fig. 6i). Moreover, SSA failed to prevent/reduce hippocampal atrophy in AAV-K174Q-injected mice (Fig. 6j), supporting the importance of ac-K174 inhibition in SSA's protective effects.

DISCUSSION

Here we report a critical role for acetylation of K174, an early pathological modification of soluble tau in AD brains, in tau accumulation and toxicity. Acetyl-mimicking tau mutant K174Q degrades slower than WT tau or K174R tau that mimics the non-acetylatable form. Hippocampal expression of K174Q, not WT or K174R tau, leads to accumulation of tau monomers that are associated with profound AD-related cognitive deficits. SSA inhibits p300, lowers ac-K174 levels in brain, and protects against behavioral deficits, hippocampal atrophy, and accumulation of NFTs in aged PS19 mice. The tau-lowering and protective effects of salicylate/SSA were diminished in neurons and mice expressing K174Q tau. Our findings point to inhibitors of tau acetylation as a novel therapeutic modality to treat tauopathies.

Levels of ac-K174 were elevated at early Braak stages in AD brains, consistent with its role in early pathogenic alteration. In PS19 mice, ac-K174 co-localized remarkably with MC1,

which is enriched in soluble tau in AD lysates and represents one of the earliest pathological tau conformations[20,21]. In addition to K174, other tau acetylation sites have been reported, including K274, K280 and K259/290/321/353 (KXGS motifs)[15,18,34–36]. Both ac-K274 and ac-K280 were found to be specifically associated with insoluble, Thioflavin-positive tau aggregates in AD and other tauopathy brains[34–36]. Although ac-K280 was implicated in deficient tau-microtubule interactions and pathological tau aggregation *in vitro*[15], its pathogenicity *in vivo* has not been established. Acetylation of KIGS motif, which appeared to be reduced in AD brains, suppresses tau aggregation and promotes microtubule binding *in vitro*[18]. However, we showed that ac-K174 had few effects on acetylation or phosphorylation of KXGS motifs, suggesting that different tau acetylation sites may exert distinct effects on tau pathogenecity.

Our findings established, for the first time, the pathogenicity of ac-tau *in vivo*. Behavioral deficits, including hyperactivity, working memory and spatial learning impairments, were observed in mice expressing K174Q tau, but not in mice expressing with similar levels of WT or K174R tau. The positive correlation of cognitive deficits with monomeric K174Q tau levels provides evidence supporting the pathogenicity of ac-K174 monomers. Tau-mediated neurodegeneration is exacerbated by ac-K174, but hippocampal atrophy was not abolished in mice expressing K174R, indicating that other mechanisms could be involved. Indeed, K174Q and K174R mutants enhance the formation of dimeric tau, which could be neurotoxic. Aberrant cell-cycle reentry induced by high levels of h-tau[25] could also contribute to neurodegeneration in mice injected with AAV-K174Q or -K174R. Our results also support a role of ac-K174 in tau homeostasis. Expressing K174Q, not K174R, leads to longer half-life in primary neurons and aberrant accumulation *in vivo*, showing that K174 acetylation *per se*, not the blockage of K174 polyubiquitination, impairs tau clearance. Interestingly, a recent mass-spec study provided clear evidence that acetylation and ubiquitination occurs on the same lysine residues, supporting an intimate relationship of these two modifications[37].

One of the main enzymes that acetylate tau is p300[14], which can be inhibited by SS/SSA, an ancient drug commonly used as an NSAID. Pharmacokinetically, SSA is quickly metabolized into its active component, salicylate. Unlike salicylate, aspirin (acetyl salicylate) elevates ac-tau in cultured neurons (not shown). SSA and aspirin had been widely used NSAIDs to treat rheumatoid arthritis and related illnesses in the past decades, presumably via inhibiting cyclo-oxygenases (COX)[38]. Interestingly, patients taking NSAIDs, including salicylate and derivatives, had a reduced risk of AD[39]. However, later trials with more specific COX-2 inhibitors failed to establish the benefits. One possible explanation is that the benefits of salicylate might involve mechanisms independent of COX2 inhibition, such as partial attenuation of p300 activity, which is identified recently as one of top dysregulated networks in AD brains[40].

The resistance of K174Q to the tau-lowering and protective effects of salicylate/SSA strongly supports that inhibition of ac-K174 as a key underlying mechanism. Treating with salicylate lowered levels of ac-tau and t-tau in primary neurons expressing WT tau, but not in those expressing K174Q tau. SSA lowered ac-K174 and t-tau, and protects against hippocampal atrophy in PS19 mice, but failed to reduce tau or to restore hippocampal

volume in AAV-K174Q-injected mice. Other mechanisms are likely to be involved as well. For example, salicylate/SSA could also exert protection by enhancing autophagy via activation of adenosine monophosphate–activated protein kinase (AMPK)[41]. The marked reduction of NFTs induced by SSA could be due to activation of autophagy. However, we did not observe significant LC3-II levels in SSA- vs. veh-treated PS19 brains (Supplementary Fig. 9). More comprehensive analyses are needed to fully address the involvement of autophagy. SSA-induced AMPK activation could also lead to p300 inhibition and degradation indirectly[42,43]. p300 is also critical for NF-κB activation and glial inflammatory responses[44,45]. We examined microgliosis or astrogliosis and observed no effects by SSA treatment, arguing against anti-inflammation as one of the main protective mechanisms (Supplementary Fig. 10).

Our study provides first proof-of-principle evidence that partial p300 inhibitor could be used to treat tauopathies. Since p300 is important for many biological functions, completely inhibiting it could cause serious side effects. However, a recent study showed that p300 activity is aberrantly elevated in AD brains[40]. Identified as one of the top dysregulated pathways in AD, aberrantly activated p300 could underlie hyperacetylation of tau in tauopathies[40]. In moderate and severe AD cases, p300 activities were significantly higher in the CA1 region, where activated p300 and p-tau were colocalized[40]. p300 activity was also elevated in aged PS19 brains. Thus, partially inhibiting p300 could normalize its aberrant activation and suppress hyperacetylation of its substrates, including tau. Indeed, the remarkable protection of SSA against tau-mediated cognitive deficits and degeneration is unprecedented and could have important clinical implications. Even after disease onset in PS19 mice, SSA treatment improved spatial memory, reduced NFT formation, and abolished hippocampal atrophy, which is associated with increased risk for conversion from mild cognitive impairment to AD[46–48]. Importantly, the human equivalent dose of 225 mg/kg in the current study is ~1350 mg/day for a 75 kg person[49], lower than the dose typically prescribed to human patients (3000 mg/day). Our study supports clinical evaluation of SSA and its derivatives as therapies in human tauopathies.

ONLINE METHODS

Primary Antibodies and Other Reagents

Monoclonal antibodies: Tau5 (AHB0042, Life Technologies), HT7 (MN1000, Thermo Scientific), Tau12 (MAB2241, EMD Millipore), 12E8 (Prothena Biosciences), PHF-1 (a kind gift from Dr. Peter Davies), MC-1 (a kind gift from Dr. Peter Davies), AT-8 (MN1020, Thermo Scientific), anti-GAPDH (MAB374, Millipore), anti-GFAP (MAB3402, Millipore), anti-CD68 (MCA1957GA, Serotec), anti-LC3 (M152-3, MBL), anti-histone H2B (#2934, Cell Signaling). *Polyclonal antibodies*: anti-HA (#3724, Cell Signaling), K48-linkage specific polyubiquitin antibody (#4289, Cell Signaling), anti-KIGS antibody (a kind gift from Dr. Leonard Petrucelli), anti-histone H3 (acetyl K18) antibody (ab1191, Abcam), anti-histone H3 antibody (ab1791, Abcam), anti-histone H2B (acetyl K12/K15) antibody (ab1759, Abcam), anti-histone H2A (acetyl K5) (ab1764, Abcam), anti-histone H2A (ab18255, Abcam). *Expression plasmids*: For expression in HEK293T cells, cDNA encoding WT, K163R, K174R, K274R, K280R, K369R, K174Q, or K274Q hTau was

cloned into pcDNA3.1 vector (Invitrogen). For expression in primary neurons, cDNA encoding WT, K174Q or K174R hTau was cloned into lentiviral FUGW vectors. *Chemicals*: MG-132 (Sigma), Cycloheximide (Sigma, St. Louis, MO), DMSO (Sigma), IU1-47 (a kind gift from Dr. Daniel Finley). Salicylate (sodium salicylate) was purchased from Sigma-Aldrich. Salsalate tablet (75% purity) was from Amneal Pharmaceuticals (Glasgow, KY).

Immunoprecipitation for HPLC-ESI-MS/MS and Western Blots

Immunoprecipitation was performed essentially according to the manufacturer's protocol: Pierce Direct IP Kit (Thermo Scientific). Briefly, antibody (monoclonal anti-Tau; ab80579, Abcam) was immobilized onto agarose gel with sodium cyanoborohydride. Then, brain homogenates lysed in RIPA buffer were applied to antibody-conjugated column and rotated overnight at 4°C. Samples were washed four times. Elution was performed in low pH elution buffer (pH 2.8), with neutralizing TRIS buffer (pH 9.5) in the collection tubes.

ESI-QqTOF Mass Spectrometric Analyses

Gel bands were manually excised out of the gel. Then, the gel spots were destained and dehydrated with acetonitrile. Subsequently, the proteins were reduced with 10 mM DTT at 60°C for 30 min, alkylated with 100 mM iodoacetamide (37°C, 45 min) and incubated with 250 ng sequencing grade trypsin (Promega) at 37°C overnight. The proteolytic peptide mixtures obtained after tryptic digestion were analyzed by reversed-phase nano-HPLC-ESI-MS/MS with an Eksigent nano-LC 2D HPLC system (Eksigent), which was directly connected to a quadrupole time-of-flight (QqTOF) QSTAR Elite mass spectrometer (AB SCIEX). Briefly, peptides were applied to a guard column (Dionex) and washed with the aqueous loading solvent (2% solvent B in A, flow rate: 20 μL/min) for 10 min. Subsequently, samples were transferred onto the analytical C18-nanocapillary HPLC column (Dionex) and eluted at a flow rate of 300 nL/min for most samples with a linear gradient 2–80% solvent B in A over 85 min. Solvents were prepared as follows, mobile phase A: 2% acetonitrile/98% of 0.1% formic acid (v/v) in water, and mobile phase B: 98% acetonitrile/2% of 0.1% formic acid (v/v) in water. Electrospray-mass spectra (ESI-MS) and tandem mass spectra (ESI-MS/MS) were recorded in positive-ion mode with a resolution of 12,000–15,000 FWHM. For collision-induced dissociation tandem mass spectrometry (CID-MS/MS), the mass window for precursor ion selection of the quadrupole mass analyzer was set to ± 1 *m/z*. The synthetic acetylated peptide IPA**Kac**TPPAPK (from ThermoFisher Scientific/Pierce Biotechnology, Rockford, IL) for mass spectrometric comparison was analyzed by reverse-phase HPLC-ESI-MS/MS with anEksigent Ultra Plus nano-LC 2D HPLC system connected to a quadrupole time-of-flight TripleTOF 5600 mass spectrometer (AB SCIEX) as described[50]. Database searches were performed using Protein Pilot Software 4.5 revision 1656 (AB SCIEX) using the Paragon Algorithm 4.5.0.0.1654 developed by AB SCIEX[51] or an in-house Mascot server version 2.3.02.[52]. Peptides containing posttranslational modifications were manually inspected based on an adaptation of previously published criteria.

Western Blots

Cells or human or mouse brain tissues were homogenized in RIPA buffer containing protease inhibitor cocktail (Sigma), 1 mM phenylmethyl sulfonyl fluoride, phosphatase inhibitor cocktail (Sigma), 5 mM nicotinamide (Sigma), and 1 μM trichostatin A (Sigma). After sonication, lysates from human or mouse brain were centrifuged at 170,000 g at 4°C for 15 min and 18,000 g at 4°C for 15 min. Supernatants were collected and protein concentrations were determined by the Bradford assay (Bio-Rad). The same amount of proteins were resolved on a 4–12% SDS-PAGE gel (Invitrogen), transferred to nitrocellulose membrane (GE Healthcare), and probed with appropriate antibodies. Bands in immunoblots were visualized by enhanced chemiluminescence (Pierce) and quantified by densitometry and ImageJ software (NIH).

Purification of GST Fusion Proteins and In Vitro Acetylation

For purification of GST fusion proteins, h-tau 2N4R coding sequence was subcloned into pGEX-4T-1 bacterial expression vector (Sigma) and transformed in BL21 (DE3) strain. After induction with 100 μM isopropyl β–D-1-thiogalactopyranoside, cells were harvested and sonicated in phosphate buffered saline with 1 mM EDTA, 0.5% TritonX-100, and protease inhibitor cocktail (Sigma). GST tagged tau or p300 proteins were purified by glutathione-agarose beads (Genscript). In vitro acetylation reactions were performed essentially as described[53] with minor modifications. In brief, 1 μg of recombinant h-tau, 2 nM acetyl CoA (Sigma), and 100 ng of purified GST-p300 in acetylation buffer (50 mM HEPES, pH 8.0, 10% glycerol, 1 mM dithiothreitol (DTT), and 10 mM Na butyrate) were incubated for 2 h at 30°C with constant shaking. Reactions were stopped by an addition of 2× LDS sampling buffer (Invitrogen), followed by SDS-PAGE and western blot analyses.

Primary Neuronal Cultures and Viral Infections

Mouse primary neurons were cultured from genetically modified pups. To generate $p300^{F/F}$ neurons, cortices of neonatal pups from $p300^{F/F}$ homozygotes breeding ($p300^{F/F}$ mice were a kind gift of Dr. Paul Brindle (St. Jude Hospital, Memphis, TN, USA)) on postnatal day 0 or 1, and dissociated and plated as described previously[52]. All other experiments using primary neuronal cultures were derived from neonatal rats due to the higher yield. Briefly, cortices of Sprague-Dawley rat pups (Charles River Laboratories) were dissociated on postnatal day 0 or 1. Purified mouse or rat cells were plated at 160,000 cells/ml in Neurobasal medium supplemented with B27 (Invitrogen) on poly-ornithine-coated plates. Lentivirus was generated, purified, and used for infection as described[54]. Recombinant lentivirus was produced by cotransfection of the shuttle vector (pRRL), two helper plasmids, delta8.9 packaging vector, and VSV-G envelope vector into 293T cells and purified by ultracentrifugation[52]. Viral titers were measured by p24 enzyme-linked immunosorbent assays at the Gladstone-UCSF Laboratory of Clinical Virology. AAV1-WT, AAV1-K174Q and AAV1-K174R tau with CMV-β-actin promoter were generated and purified by GENEDETECT (Auckland 0600, New Zealand). Primary neuronal cultures were infected with either equal amount (~3–5 × 10^7 PFU) of lentiviral vectors or AAV1 (~5 × 10^8 genomic particles) expressing tau WT and mutants at days in vitro (DIV) 3–5. Once available, tau-expressing AAV1 vectors were used in later experiments since they exhibited

less toxicity than lentiviral vectors. If necessary, viruses were diluted with conditioned medium for infection. All drug treatments and analyses were performed at DIV 8–11.

RNA Isolation and Quantitative Reverse Transcription (RT)-PCR

Brain hippocampi from AAV-Tau injected mice were dissected and homogenized with a 21G needle in RLT buffer with 1% β-mercaptoethanol. RNA was isolated with the RNeasy mini-kit (Qiagen), and the remaining DNA was removed by incubation with RNase-free DNase (Ambion). Purified messenger RNA was then converted to complementary DNA by the TaqMan reverse transcription (RT) kit (Applied Biosystems). Quantitative RT-PCR was performed on the ABI 7900 HT sequence detector (Applied Biosystems) with SYBR Green PCR master mix (Applied Biosystems). The average value of three replicates of each sample was expressed as the threshold cycle (C_t), at which the fluorescence signal starts to increase rapidly. Then, the difference (ΔC_t) between the C_t value for h-tau and the C_t value for mouse GAPDH ($\Delta C_t = C_t$(human tau)-C_t(GAPDH)) was calculated for each sample. The relative levels of gene expression for each sample was determined by $2^{-\Delta C_t}$ and expressed as the-fold change. The following primers were used for quantitative RT-PCR: h-tau (forward, 5′-GTTGGGGGACAGGAAAGATCAG-3′; reverse, 5′-CCGGGAGCTCCCTCATC-3′), mouse GAPDH (forward, 5′-GGGAAGCCCATCACCATCTT-3′; reverse, 5′-GCCTTCTCCATGGTGGTGAA-3′).

In Vitro Tau Aggregation Assay

Site-directed mutagenesis was used to generate K174Q and K174R mutants of the 0N4R tau isoform in a pET28a vector. WT and mutant proteins were expressed in *E. coli* and purified by heat denaturation, followed by cation exchange chromatography[55]. For aggregation assays, tau proteins (10 μM) were incubated in assay buffer: D-PBS, pH 7.2 (Invitrogen), 2 mM $MgCl_2$, 1 mM DTT. Heparin (Santa Cruz, MW 6,000–25,000) was reconstituted in assay buffer then added at a final concentration of 44 μg/ml to induce tau aggregation. The aggregation assay was carried out at 37°C with agitation. When monitoring aggregation kinetics, Thioflavin T (ThT, Sigma) was dissolved in assay buffer and included in the reaction at a final concentration of 10 μM. The Thioflavin T fluorescence intensity was measured in a Spectramax M5 reader (Molecular Devices) set to excitation (444 nm)/emission (485 nm) with an emission cutoff of 480 nm. Samples were read in a 384-well plate format, in quadruplicate, at 37°C, with reads every 5 min and agitation between reads. Control reactions containing WT or mutant tau without heparin were included as baseline readings in each experiment. Baseline subtracted kinetic data was fit to the Gompertz equation[56,57] $y = Ae^{-e^{(t-t_i)/b}}$ (1) where y = the fluorescence at time t, A is the maximum signal/amplitude of curve, t_i is the inflection point, t_i-b = lag time, and $b = 1/k_{app}$ where k_{app} is the apparent elongation rate constant. Amplitude values are represented relative to WT controls for each experiment to adjust for day to day variations in absolute ThT signal intensity.

Mice

Mice were assigned into gender- and age-matched treatment groups in a randomized manner. The sample size for each experiment was determined based on previous experience

with each of the animal models used. For AAV-Tau injection experiments, male (C57BL/6) mice at 2–3 months of age were purchased from the Jackson Laboratory and housed in a pathogen-free barrier facility at UCSF with a 12-h light/dark cycle and ad libitum access to food and water. All behavior experiments were performed during daylight hours. All animal procedures were carried out under University of California, San Francisco, Institutional Animal Care and Use Committee-approved guidelines. For SSA treatment experiment, both female (first cohort) and male (second cohort) PS19 mice were purchased from the Jackson Laboratory. The mice were housed in a conventional facility at Stanford University (Palo Alto, CA) with a 12-h light/dark reverse cycle and ad libitum access to food and water. All behavior experiments of PS19 mice were performed during daylight hours and carried out under Stanford University School of Medicine, Institutional Animal Care and Use Committee-approved guidelines.

Stereotaxic Injections

Mice were anesthetized with avertin (250 mg/kg) by intraperitoneal injection, and secured on a stereotaxic frame (Kopf Instruments). Equal amount (~ 3 X 10^9 genomic particles) of AAV1 expressing tau WT, tau K174Q and tauK174R mutant were injected into dentate gyrus of 3-month-old mice by stereotaxic injection at a rate of 0.5 μl/min. The following coordinates were used (anterior-posterior -2.1, medial-lateral ±1.7, dorsal-ventral -2.1).

Oral Gavage

Oral gavage was performed either at the animal facility at Stanford University (for PS19 mice) or at Preclinical Therapeutics Core, UCSF Helen Diller Family Comprehensive Cancer Center (for AAV-injected wildtype mice). Each group was assigned for a different treatment in a semi-random manner. The dosers were blinded to the genotypes or of the mice or vectors injected. In the first PS19 cohort, two groups of 8–9-month-old PS19 female mice and one group of NTG littermate controls were used in the study. PS19 mice were administered with vehicle (PEG400: Tween 20 (4:1)) or SSA (225 mg/kg body weight) for 7 days a week via daily single oral gavage ingestion (100 μl solution per 10 g body weight). NTG littermates were administered with vehicle. Dosing was administered for 5 weeks before the initiation of the behavioral tests, and continued until the mice were sacrificed (60 days in total). In the repeat cohort, two groups (vehicle and SSA) of 7–8-month-old PS19 male mice and two groups (vehicle and SSA) of NTG littermate controls were used. The vehicle used in cohort 2 contained PEG-400 (10%, v/v), Tween-80 (10%, v/v), Labrasol (10%, v/v), hydroxpropyl beta-cyclodextrin (20%, w/v), sodium phosphate (mono-basic), sodium phosphate (dibasic) and sodium chloride. Dosing was administered for about 60 days before the initiation of the MWM test, and continued until the mice were sacrificed (86 days in total). Body weights of animals were monitored once a week. In AAV-TauK174Q injected cohort, 3-month-old C57BL/6 mice were injected with AAV-TauK174Q. After 2 months of post-injection, mice were daily treated either with vehicle or SSA (225 mg/kg body weight) for 6 weeks until the mice were sacrificed.

Hippocampal Volume Quantification and Immunostaining/Gallyas Silver Staining

Experimenters were blind to the genotypes or treatment of the mice. For quantification of hippocampal volume, mice hemibrains were cut at 30 μm coronally, and all hippocampi,

including sections, were collected. Brain sections were mounted on microscope slides (Fisher Scientific) in an anterior to posterior order, starting from the section where the hippocampal structure first becomes visible (1st section) to the section where hippocampal structure just disappears (last section). Mice with missing sections were excluded from the analyses, a pre-established criterion. Mounted brain sections were dried at room temperature for 24 h and stained with cresyl violet (nissl staining). After being defatted for 15 min in 100% xylene and 10 min in 100% ethanol, followed by rehydration, sections were stained in 0.1% cresyl violet solution and mounted in DePeX mounting medium (VWR). Images were acquired with a Keyence BZ-9000 microscope. Hippocampal volume was estimated using ImageJ (NIH) Volumest plugin (http://lepo.it.da.ut.ee/~markkom/volumest/). Usually 10–12 hippocampal-containing sections were used for each analysis. For immunostaining, floating sections were permeabilized and incubated in blocking solution (10% normal goat serum in 0.3% Triton X-100 TBST) at room temperature for 1 h. Anti-HT7 (MN1000, Thermo Scientific) were incubated, and immunoreactive structures were detected with either Alexa Fluor 488- or 555-secondary antibodies (Invitrogen). For AC312 immunostaining, to reduce the non-specific nuclear staining, the antibody was pre-absorbed by acetone Tau KO mice brain powder. Antigen retrieval was first performed by heating the sections in 10 mM citric acid at 90°C for 30 min. Sections were then incubated with brain powder pre-absorbed AC312 and AT8 (Fisher) or MC1. After overnight incubation, the sections were incubated with secondary antibodies including Cy3-labeled donkey anti-rabbit IgG (Jackson ImmunoResearch) and fluorescein-labeled goat anti-mouse IgG (Vector Laboratories). All images were acquired by DM5000B microscope (Leica) or CSU-W1 spinning disk confocal microscope (Nikon) with 60× oil immersion objective lens and analyzed by either Micro-Manager software (UCSF) or imageJ software (NIH). For orthogonal images, images were collected as Z stacks with size of Z step as 0.15 microns and total 2.5 microns stacked images were rendered for orthogonal view with Image J software. Gallyas silver staining was performed as described[58]. Briefly, sections were placed in 5% periodic acid followed by alkaline silver iodide solution and developer solution. After washing with acetic acid and water, they were placed in 0.1% gold chloride, followed by sodium thiosulphate solution, washed and counterstained in 0.1% nuclear fast red. For quantification, three sections were analyzed by bright light digital microscopy with an Olympus BX41 microscopy. Four fields per section and brain region were analyzed at 400X, and silver-positive neuronal cell bodies and neurites were estimated and averaged per 0.1 mm^2.

PK Analyses of SSA and Salicylic Acid (SA) in Brain and Plasma

SSA was administered to C57B6 mice of both males and females via oral garage as a single bolus dose. Mice were sacrificed at predetermined time points and plasma and brain tissue samples were harvested for analysis by PPL labs (Redwood City, CA). SSA and its metabolite SA were measured simultaneously using oxopropanoyloxy benzoic acid as an internal standard solution[59]. To extract SSA/SA from brain, 200 μl of 50% acetonitrile in 0.1% formic acid was added to 30–50 mg of cortical tissue, followed by homogenization and vortexing. After addition of 200 μl of the internal standard solution, the samples were centrifuged and the supernatants were transferred for injection. To measure SSA/SA in the plasma, 10 μl of plasma samples were mixed with 90 μl H_2O and 100 μl of Internal Standard Solution, followed by centrifugation and injection. The HPLC was performed in C18

column, following a gradient program (10–90% acetonitrile in 6 min) with a flow rate of 0.4 ml/min. The injection volume is ~ 5 μl. The mass spectrometry analyses were perform on 3200 Q TRAP system (AB SCIEX, Framingham, MA) using MQL algorithm.

Human Tau ELISA

High-binding black 96-well plates (Costar, Corning, NY) were coated with 2.5 μg/ml HT7 capture antibody diluted in Tris-buffered saline (TBS), pH 8. After incubating at 4°C overnight, plates were blocked with 3% bovine serum albumin, followed by TBST wash (TBS containing 0.05% Tween-20). Plates were washed with TBST before the addition of 50 μl per well diluted PS19 mice brain lysates and h-tau441, diluted in a TBS assay buffer, pH 8. Assay plates containing samples and standards were incubated overnight at 4°C while shaking. Alkaline phosphatase (AP)-conjugated Tau5 antibody was diluted into assay buffer before being added to the assay plate (50 μl per well) to co-incubate with PS19 mice brain lysates and htau441 standards for 1 h at room temperature while shaking. Plates were washed with TBST before being developed using alkaline phosphatase substrate (T2214; Applied Biosystems, Foster City, CA). Luminescence counts were measured using SpectraMax M5 (Molecular Devices, Sunnyvale, CA). Log-transformed luminescence counts from individual samples were interpolated to concentration using a third-order polynomial fit to the respective standards (GraphPad Prism 5.00, GraphPad Software, San Diego, CA). PS19 mice tau levels were plotted after correction for dilution factor.

Morris Water Maze

Experimenters were blind to the genotypes or treatments of the mice for all behavioral analyses. The water maze consisted of a pool (122 cm in diameter) containing opaque water (20 ± 1°C) and a platform (14 cm in diameter) submerged 1.5 cm under the water. Hidden platform training (days 1–5) consisted of 10 sessions (two per day, 2 h apart), each with three trials. The mouse was placed into the pool at alternating drop locations for each trial. A trial ended when the mouse located the platform. The maximum trial time was 60 s per trial. Mice that failed to find the platform within 60 s trial were led to it and placed on it for 15 s. After the initial learning task, a reversal learning protocol (days R1–R4; two per day, 2 h apart) was conducted for the same mice. The hidden platform was moved to the opposite quadrant for reversal learning. For probe trial, 48 h after the final reversal training trial, mice were returned to the pool with a new drop location in the absence of hidden platform. Performance was measured with an EthoVision video-tracking system (Noldus Information Technology). Visible platform training, where the platform was cued with a mounted black-and-white striped mast, was conducted for four trials after completion of probe trials. The pre-established exclusion criterion is that mice that floated or did not swim would be excluded from analysis.

Small Y-Maze

Mice were placed in the center of a small Y-maze (arm length: 15 cm) and spontaneous alternation was recorded in a single continuous 6 min trial by a live observer. Each of the three arms was designated a letter A–C, and entries into the arms were recorded. The percent of spontaneous alternation was calculated over the total number of entries possible. The apparatus was cleaned with 70% ethanol between trials.

Open Field Test

Mice were placed individually into brightly lit automated activity cages equipped with rows of infrared photocells interfaced with a computer (San Diego Instruments). After a 1-min adaptation period, open field activity was recorded for 20 min. Recorded beam breaks were used to calculate active times, path lengths, rearing times, and rearing events. After behavioral testing, the apparatus was cleaned with 70% ethanol between trials.

Fixed Location Dry Maze (also called DMP dry maze[35])

Experiments were performed at animal facility at Stanford University. Mice were housed at a standard temperature (22 ± 1 °C), in a reverse light-controlled environment (lights off from 8:30 am to 8:30 pm) with ad libitum access to food and water. Animals are group-housed with minimal enrichment such as shelter (paper towel tubes and nestlets). The experimenter remained blinded to the experimental groups throughout the entire study. A custom built dry maze was used, which is a 122-cm diameter circular platform with 40 escape holes (5 cm in diameter). The target escape tube is attached to one of these holes; all other holes except the target escape hole are left open. High overhead lighting (~750 lux) and air turbulence created by fans are used as aversive stimuli to encourage the animals to seek out the target escape hole. All aversive stimuli are turned off when the mouse enters the target escape hole. Visual cues are provided around the maze for navigation. The subjects are monitored by a video tracking system directly above maze, and the parameters are measured using the computer software Ethovision. Subjects are given four trials to find the target escape hole with a 2-min inter-trial-interval. Each trial is 90 s long. Animals that could not find the escape hole were led by the experimenter and allowed to enter the target escape hole. After each trial, the apparatus was cleaned with 1% Virkon to eliminate odor cues. After 2 days of training and 3 days of learning, mice are tested in a probe trial. During the probe, the escape tube is removed from the maze and the mice are allowed to explore the maze. Time in each quadrant is recorded and memory is assessed by the time spent in the target quadrant versus the other three quadrants.

Statistical Analysis

Data were analyzed with GraphPad Prism v.5 (GraphPad) or STATA12 (StataCorp LP). Differences between means were assessed with paired or unpaired Student's *t* test, one-way or two-way analysis of variance, followed by post hoc testing of all pairwise comparisons among genotypes (with *Tukey-Kramer* correction or Dunnett's test for one-way ANOVA and Bonferroni correction for two-way ANOVA), or by mixed effects model, as indicated. Pearson's correlation coefficients were used to quantify the linear relationship between two variables. The Shapiro-Wilk test of normality was applied to all data sets, and in cases where the data did not demonstrate a normal distribution, non-parametric tests were used to analyze statistical differences. The Mann-Whitney test was used for unpaired t-tests, the Wilcoxon matched pairs test was used for paired comparisons, and the Kruskal-Wallis test was used for ANOVAs. Multilevel mixed-effects linear regression model fit using STATA12 were used to compare learning curves in MWM and fixed location dry maze; random intercepts and linear time slopes for each mouse were taken into account for the correlation among repeated observations. Outliers are pre-established as data outside of

mean ± 2SD. All samples or animals were included for statistical analysis unless otherwise noted in pre-established criteria.

Supplementary Material

Refer to Web version on PubMed Central for supplementary material.

Acknowledgments

We thank V. Haroutunian (The Mount Sinai School of Medicine, New York) for human brain samples, B. Hann and J. Freimuth for oral gavage, L. Petrucelli (Mayo Clinic, Florida) for ac-KIGS antibody, Prothena Biosciences for 12E8 antibody, R. Ponnusamy and N. Devidze for advice on behavioral analyses, D. Song for PK analyses (PPL labs, Redwood City), M. Finucane and S. Liu for advice on statistical analyses, L. Mucke and S. Meada for insightful discussions, L. Grinberg for technical advice on pathological analyses, C. Brennecka, G. Howard, and S. Ordway for editorial review, J. Carroll and G. Maki for graphics assistance, and E. Nguyen for administrative assistance. This work was supported by a grant from Tau Consortium (to L.G.), and US National Institute of Health (1R01AG036884 and R01AG030207 to L.G.). We acknowledge the support of National Institute of Health to LME (NIH NS40251 and NIH NS062413), and instrumentation from the NCRR shared instrumentation grant S10 RR024615 (BWG) and AB SCIEX for evaluation of the TripleTOF 5600 at the Buck Institute.

References

1. Ludolph AC, et al. Tauopathies with parkinsonism: clinical spectrum, neuropathologic basis, biological markers, and treatment options. Eur J Neurol. 2009; 16:297–309. [PubMed: 19364361]
2. Cairns NJ, et al. Neuropathologic diagnostic and nosologic criteria for frontotemporal lobar degeneration: consensus of the Consortium for Frontotemporal Lobar Degeneration. Acta neuropathologica. 2007; 114:5–22. [PubMed: 17579875]
3. Braak H, Braak E. Neuropathological stageing of Alzheimer-related changes. Acta Neuropathol Berl. 1991; 82:239–259. [PubMed: 1759558]
4. Lasagna-Reeves CA, et al. Identification of oligomers at early stages of tau aggregation in Alzheimer's disease. FASEB journal : official publication of the Federation of American Societies for Experimental Biology. 2012; 26:1946–1959. [PubMed: 22253473]
5. Ren Y, Sahara N. Characteristics of tau oligomers. Frontiers in neurology. 2013; 4:102. [PubMed: 23882258]
6. Maeda S, et al. Increased levels of granular tau oligomers: an early sign of brain aging and Alzheimer's disease. Neuroscience research. 2006; 54:197–201. [PubMed: 16406150]
7. Lasagna-Reeves CA, et al. Tau oligomers impair memory and induce synaptic and mitochondrial dysfunction in wild-type mice. Molecular neurodegeneration. 2011; 6:39. [PubMed: 21645391]
8. Berger Z, et al. Accumulation of pathological tau species and memory loss in a conditional model of tauopathy. The Journal of neuroscience : the official journal of the Society for Neuroscience. 2007; 27:3650–3662. [PubMed: 17409229]
9. Santacruz K, et al. Tau suppression in a neurodegenerative mouse model improves memory function. Science. 2005; 309:476–481. [PubMed: 16020737]
10. Sydow A, et al. Reversibility of Tau-related cognitive defects in a regulatable FTD mouse model. Journal of molecular neuroscience : MN. 2011; 45:432–437. [PubMed: 21822709]
11. Wang Y, Mandelkow E. Degradation of tau protein by autophagy and proteasomal pathways. Biochemical Society transactions. 2012; 40:644–652. [PubMed: 22817709]
12. Lee BH, et al. Enhancement of proteasome activity by a small-molecule inhibitor of USP14. Nature. 2010; 467:179–184. [PubMed: 20829789]
13. Tai HC, et al. The synaptic accumulation of hyperphosphorylated tau oligomers in Alzheimer disease is associated with dysfunction of the ubiquitin-proteasome system. The American journal of pathology. 2012; 181:1426–1435. [PubMed: 22867711]
14. Min SW, et al. Acetylation of tau inhibits its degradation and contributes to tauopathy. Neuron. 2010; 67:953–966. [PubMed: 20869593]

15. Cohen TJ, et al. The acetylation of tau inhibits its function and promotes pathological tau aggregation. Nature communications. 2011; 2:252.
16. Kim GW, Yang XJ. Comprehensive lysine acetylomes emerging from bacteria to humans. Trends in biochemical sciences. 2010
17. Mandelkow EM, Mandelkow E. Biochemistry and cell biology of tau protein in neurofibrillary degeneration. Cold Spring Harbor perspectives in medicine. 2012; 2:a006247. [PubMed: 22762014]
18. Cook C, et al. Acetylation of the KXGS motifs in tau is a critical determinant in modulation of tau aggregation and clearance. Human molecular genetics. 2013
19. Yoshiyama Y, et al. Synapse loss and microglial activation precede tangles in a P301S tauopathy mouse model. Neuron. 2007; 53:337–351. [PubMed: 17270732]
20. Jicha GA, Bowser R, Kazam IG, Davies P. Alz-50 and MC-1, a new monoclonal antibody raised to paired helical filaments, recognize conformational epitopes on recombinant tau. Journal of neuroscience research. 1997; 48:128–132. [PubMed: 9130141]
21. Weaver CL, Espinoza M, Kress Y, Davies P. Conformational change as one of the earliest alterations of tau in Alzheimer's disease. Neurobiology of aging. 2000; 21:719–727. [PubMed: 11016541]
22. Yeung F, et al. Regulation of the mitogen-activated protein kinase kinase (MEK)-1 by NAD-dependent deacetylases. Oncogene. 2014
23. Wang B, et al. Microtubule acetylation amplifies p38 kinase signalling and anti-inflammatory IL-10 production. Nature communications. 2014; 5:3479.
24. Zhao Y, et al. p300-dependent acetylation of activating transcription factor 5 enhances C/EBPbeta transactivation of C/EBPalpha during 3T3-L1 differentiation. Molecular and cellular biology. 2014; 34:315–324. [PubMed: 24216764]
25. Jaworski T, et al. AAV-tau mediates pyramidal neurodegeneration by cell-cycle re-entry without neurofibrillary tangle formation in wild-type mice. PloS one. 2009; 4:e7280. [PubMed: 19794916]
26. Lecourtier L, et al. Intact neurobehavioral development and dramatic impairments of procedural-like memory following neonatal ventral hippocampal lesion in rats. Neuroscience. 2012; 207:110–123. [PubMed: 22322113]
27. Takeuchi H, et al. P301S mutant human tau transgenic mice manifest early symptoms of human tauopathies with dementia and altered sensorimotor gating. PloS one. 2011; 6:e21050. [PubMed: 21698260]
28. Kasper LH, et al. CBP/p300 double null cells reveal effect of coactivator level and diversity on CREB transactivation. The EMBO journal. 2010; 29:3660–3672. [PubMed: 20859256]
29. Kasper LH, Qu C, Obenauer JC, McGoldrick DJ, Brindle PK. Genome-wide and single-cell analyses reveal a context dependent relationship between CBP recruitment and gene expression. Nucleic acids research. 2014; 42:11363–11382. [PubMed: 25249627]
30. Jin Q, et al. Distinct roles of GCN5/PCAF-mediated H3K9ac and CBP/p300-mediated H3K18/27ac in nuclear receptor transactivation. The EMBO journal. 2011; 30:249–262. [PubMed: 21131905]
31. Kouzarides T. Chromatin modifications and their function. Cell. 2007; 128:693–705. [PubMed: 17320507]
32. Yoshiyama Y, Kojima A, Ishikawa C, Arai K. Anti-inflammatory action of donepezil ameliorates tau pathology, synaptic loss, and neurodegeneration in a tauopathy mouse model. Journal of Alzheimer's disease : JAD. 2010; 22:295–306. [PubMed: 20847440]
33. Faizi M, et al. Thy1-hAPP(Lond/Swe+) mouse model of Alzheimer's disease displays broad behavioral deficits in sensorimotor, cognitive and social function. Brain and behavior. 2012; 2:142–154. [PubMed: 22574282]
34. Grinberg LT, et al. Argyrophilic grain disease differs from other tauopathies by lacking tau acetylation. Acta neuropathologica. 2013; 125:581–593. [PubMed: 23371364]
35. Irwin DJ, et al. Acetylated tau neuropathology in sporadic and hereditary tauopathies. The American journal of pathology. 2013; 183:344–351. [PubMed: 23885714]
36. Irwin DJ, et al. Acetylated tau, a novel pathological signature in Alzheimer's disease and other tauopathies. Brain : a journal of neurology. 2012; 135:807–818. [PubMed: 22366796]

37. Morris M, et al. Tau post-translational modifications in wild-type and human amyloid precursor protein transgenic mice. Nature neuroscience. 2015; 18:1183–1189. [PubMed: 26192747]
38. Smith WL, DeWitt DL, Garavito RM. Cyclooxygenases: structural, cellular, and molecular biology. Annu Rev Biochem. 2000; 69:145–182. [PubMed: 10966456]
39. in t' Veld BA, et al. Nonsteroidal antiinflammatory drugs and the risk of Alzheimer's disease. N Engl J Med. 2001; 345:1515–1521. [PubMed: 11794217]
40. Aubry S, et al. Assembly and interrogation of Alzheimer's disease genetic networks reveal novel regulators of progression. PloS one. 2015; 10:e0120352. [PubMed: 25781952]
41. Hawley SA, et al. The Ancient Drug Salicylate Directly Activates AMP-Activated Protein Kinase. Science. 2012
42. Zhang Y, Qiu J, Wang X, Zhang Y, Xia M. AMP-activated protein kinase suppresses endothelial cell inflammation through phosphorylation of transcriptional coactivator p300. Arterioscler Thromb Vasc Biol. 2011; 31:2897–2908. [PubMed: 21940946]
43. Lim JY, Oh MA, Kim WH, Sohn HY, Park SI. AMP-activated protein kinase inhibits TGF-beta-induced fibrogenic responses of hepatic stellate cells by targeting transcriptional coactivator p300. Journal of cellular physiology. 2012; 227:1081–1089. [PubMed: 21567395]
44. Greene WC, Chen LF. Regulation of NF-kappaB action by reversible acetylation. Novartis Foundation symposium. 2004; 259:208–217. discussion 218–225. [PubMed: 15171256]
45. Lee H, et al. Ethanol selectively modulates inflammatory activation signaling of brain microglia. Journal of neuroimmunology. 2004; 156:88–95. [PubMed: 15465599]
46. Apostolova LG, et al. Conversion of mild cognitive impairment to Alzheimer disease predicted by hippocampal atrophy maps. Archives of neurology. 2006; 63:693–699. [PubMed: 16682538]
47. Kerchner GA, et al. Hippocampal CA1 apical neuropil atrophy in mild Alzheimer disease visualized with 7-T MRI. Neurology. 2010; 75:1381–1387. [PubMed: 20938031]
48. Leung KK, et al. Cerebral atrophy in mild cognitive impairment and Alzheimer disease: rates and acceleration. Neurology. 2013; 80:648–654. [PubMed: 23303849]
49. Reagan-Shaw S, Nihal M, Ahmad N. Dose translation from animal to human studies revisited. FASEB journal : official publication of the Federation of American Societies for Experimental Biology. 2008; 22:659–661. [PubMed: 17942826]
50. Schilling B, et al. Platform-independent and label-free quantitation of proteomic data using MS1 extracted ion chromatograms in skyline: application to protein acetylation and phosphorylation. Molecular & cellular proteomics : MCP. 2012; 11:202–214. [PubMed: 22454539]
51. Shilov IV, et al. The Paragon Algorithm, a next generation search engine that uses sequence temperature values and feature probabilities to identify peptides from tandem mass spectra. Molecular & cellular proteomics : MCP. 2007; 6:1638–1655. [PubMed: 17533153]
52. Perkins DN, Pappin DJ, Creasy DM, Cottrell JS. Probability-based protein identification by searching sequence databases using mass spectrometry data. Electrophoresis. 1999; 20:3551–3567. [PubMed: 10612281]
53. Pagans S, et al. SIRT1 regulates HIV transcription via Tat deacetylation. PLoS Biol. 2005; 3:e41. [PubMed: 15719057]
54. Chen J, et al. SIRT1 Protects against Microglia-dependent Amyloid-{beta} Toxicity through Inhibiting NF-{kappa}B Signaling. The Journal of biological chemistry. 2005; 280:40364–40374. [PubMed: 16183991]
55. Barghorn S, et al. Structure, microtubule interactions, and paired helical filament aggregation by tau mutants of frontotemporal dementias. Biochemistry. 2000; 39:11714–11721. [PubMed: 10995239]
56. Moore CL, et al. Secondary nucleating sequences affect kinetics and thermodynamics of tau aggregation. Biochemistry. 2011; 50:10876–10886. [PubMed: 22085312]
57. Winsor CP. The Gompertz Curve as a Growth Curve. Proceedings of the National Academy of Sciences of the United States of America. 1932; 18:1–8. [PubMed: 16577417]
58. Sun A, Nguyen XV, Bing G. Comparative analysis of an improved thioflavin-s stain, Gallyas silver stain, and immunohistochemistry for neurofibrillary tangle demonstration on the same sections. The journal of histochemistry and cytochemistry : official journal of the Histochemistry Society. 2002; 50:463–472. [PubMed: 11897799]

59. Kim SW, et al. Robust protective effects of a novel multimodal neuroprotectant oxopropanoyloxy benzoic acid (a salicylic acid/pyruvate ester) in the postischemic brain. Molecular pharmacology. 2011; 79:220–228. [PubMed: 21036874]

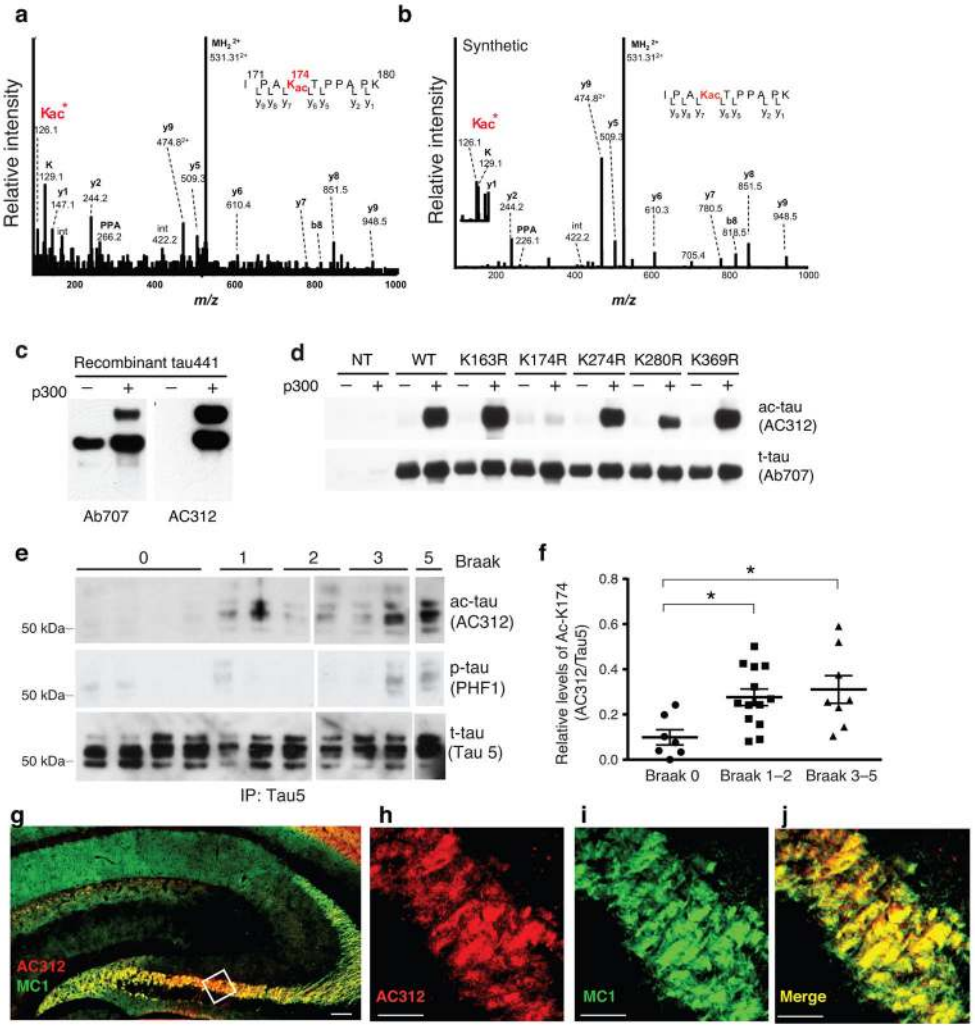

Figure 1. Tau-K174 Is Acetylated at Early Stages of AD

(**a**) ESI-MS/MS tandem mass spectra of Lys-acetylated peptide IPAK$_{Ac}$TPPAPK (residues 171–180) with a Protein Pilot confidence score of 99 obtained after trypsin digestion of immunoprecipitated Tau from AD brains. K*: Marker ion at 126.1 for acetyllysine immonium ion identification. (**b**) ESI-MS/MS tandem mass spectrum of acetyl-lysine containing synthetic peptide IPAKacTPPAPK. The corresponding Protein Pilot confidence score was 99. (**c**) Immunoblot of recombinant tau in the presence or absence of p300 showing acetyl-tau-specificity of AC312. (**d**) Immunoblot of lysates from HEK293 cells expressing tau mutants. Mutation of K174R diminished p300-induced immunoreactivity of AC312. (**e–f**) AC312-positive ac-tau (K174) signal was detected in AD brains (Braak stages 1–5). (e) Immunoblot of Tau5 immunoprecipitates with AC312 and PHF-1 antibodies. (f) Levels of ac-K174 were significantly higher at early and late Braak stages than those at Braak stage 0; n = 7 (Braak 0), n = 13 (Braak 1–2), n = 8 (Braak 3–5). * $p < 0.05$, one-way ANOVA, Tukey-Kramer post hoc analyses. See Supplementary Table-1 for the patient information. (**g–j**) AC312 immunoreactivity in the hippocampus of PS19 mice. (g) Merged image of AC312 and MC1 immunostaining at low magnification; scale bar 100 μm. (h–j)

High-magnification confocal images showing (h) AC312-positive and (i) MC1-positive tau are highly colocalized (j); scale bar 25 μm. Values are means ± SEM (f). WT, wild-type.

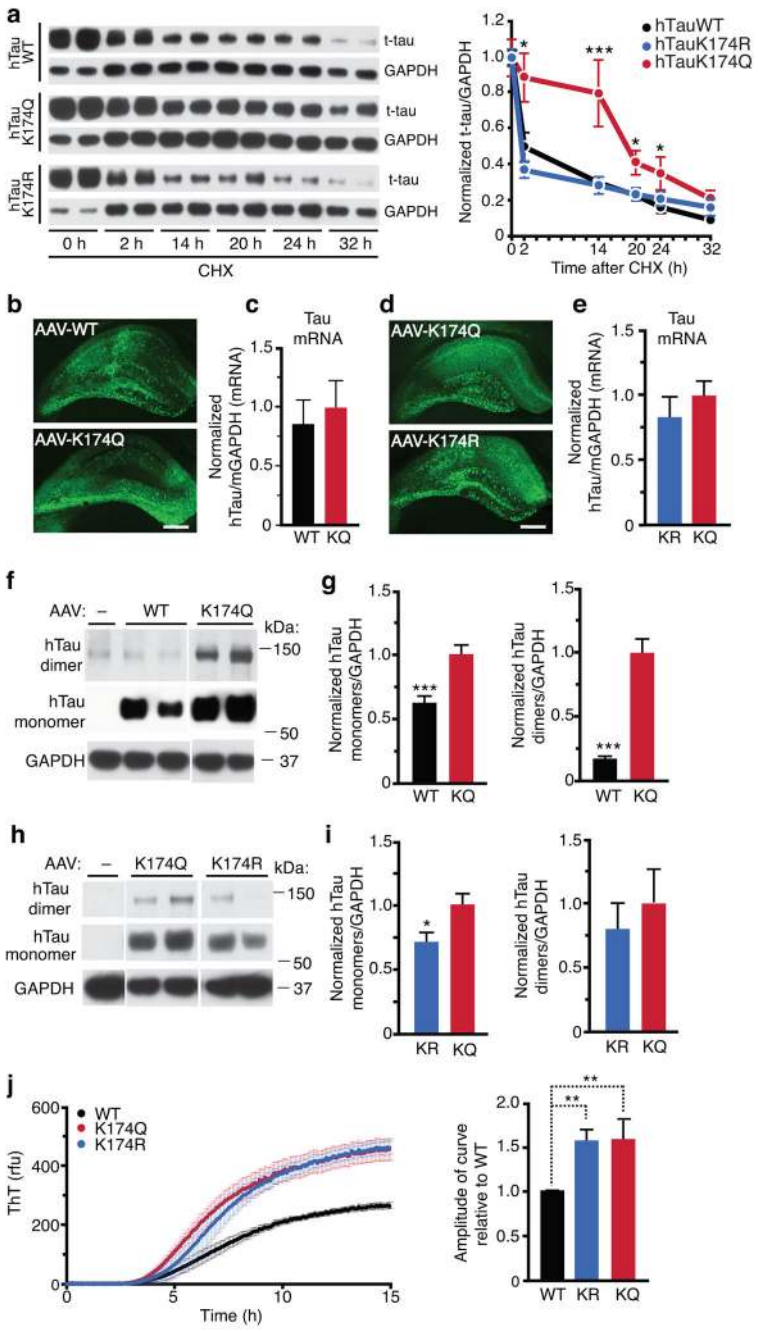

Figure 2. Acetyl-Mimic K174Q Leads to Tau Accumulation In Vitro and In Vivo

(**a**) K174Q tau had longer half-life than WT or K174R tau. Primary neurons were infected with lenti-WT, K174Q or K174R tau for four days before CHX treatment. (*left*) Representative immunoblot of WT, K174Q or K174R tau in primary neurons treated with CHX for 0–32 hours. (*right*) Quantification of WT, K174Q, or K174R tau turnover. n=15, n=8, n=8, from 4 independent experiments. Levels of tau were normalized to those of GAPDH at different time points. * $p < 0.05$, K174Q vs WT at 2, 20, or 24 h. *** $p<0.001$, at 14 h. One-way ANOVA, Tukey-Kramer post hoc analyses. (**b, d**) Representative images

showing HT7 immunostaining of hippocampus 10 days after injection of equal amounts of AAV-WT vs. K174Q tau (b), or AAV-K174Q vs. AAV-K174R tau (d). Scale bar=500 μm. (**c, e**) qRT-PCR showing similar levels of human tau mRNA are transduced three months after the infection. GAPDH was used as internal control. (c) n=10 (for WT), 12 (for K174Q). Mann-Whitney non-parametric test. (e) n=9 (for K174R and K174Q), unpaired student t-test. (**f,g**) K174Q mutation elevated levels of tau monomers and dimers. (f) Representative immunoblot with HT7 showing tau monomers and putative dimers in hippocampus injected with AAV-WT or AAV-K174Q. (g) Quantification of tau monomers (*left*) and tau dimers (*right*). n=11 (WT), n=12 (K174Q). *** $p < 0.001$, unpaired student t-test. (**h,i**) K174R mutation elevates tau dimers as K174Q, but not monomers. (h) Representative immunoblot with HT7 showing monomeric tau and putative tau dimers in hippocampus injected with AAV-K174Q or AAV-K174R tau. (i) Quantification of tau monomers (*left*) and dimers (*right*). n=9/genotype. * $p < 0.05$, unpaired student t-test. (**j**) *In vitro* aggregation analyses of recombinant WT, K174Q and K174R. (*left*) Tau aggregation kinetics was assayed by Thioflavin T fluorescence following the addition of heparin. (*right*) Amplitude of curve obtained from parameters fit to the Gompertz equation. ** $p < 0.01$, one-way ANOVA, Tukey-Kramer post hoc analyses from three independent experiments. KQ=K174Q tau, KR=K174R tau. Values are means ± SEM (a,c,e,g,i,j). WT, wild-type.

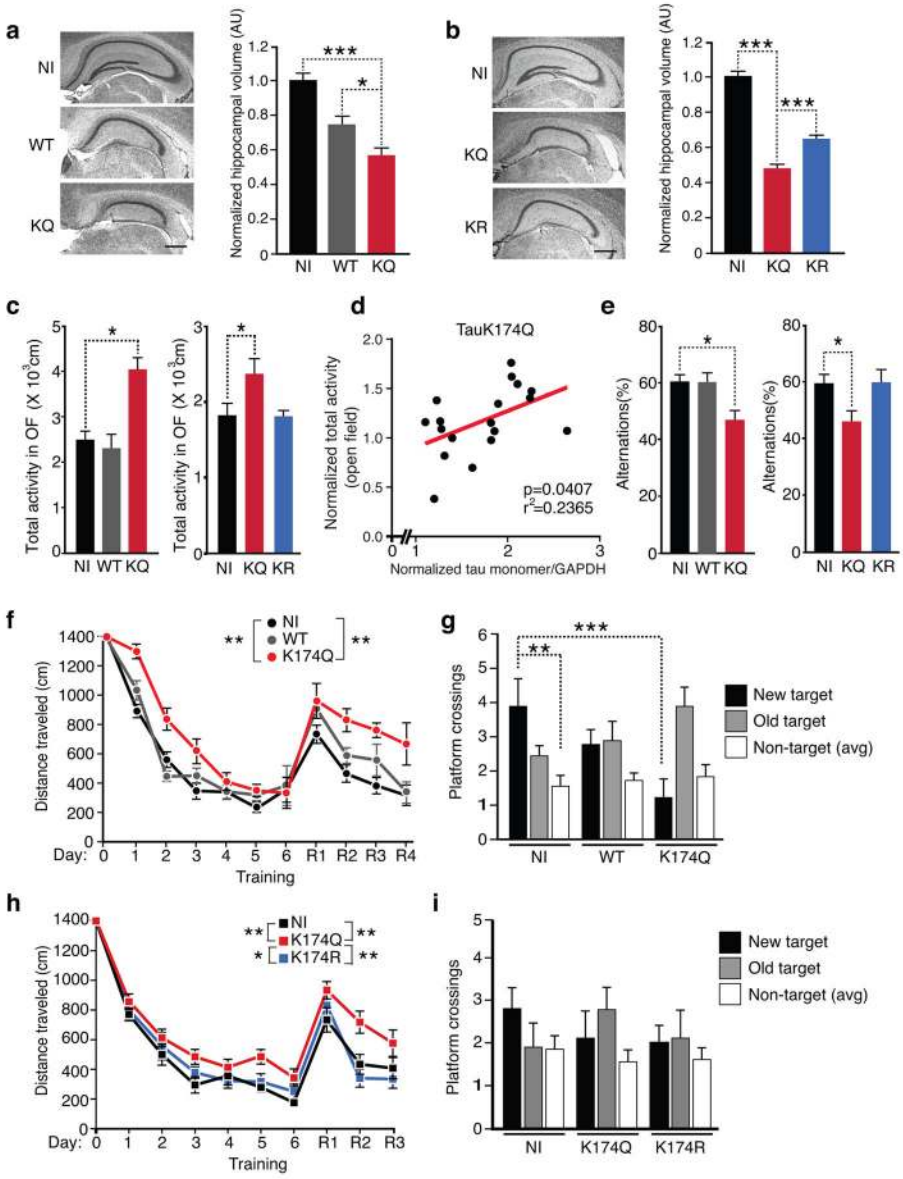

Figure 3. Expression of K174Q Tau Induces Neurodegeneration and Cognitive Deficits

(**a,b**) Expression of K174Q tau leads to more loss of hippocampal volume than WT or K174R tau. Representative nissl staining and volume quantification of hippocampus from NI (n=7), AAV-WT tau (WT, n=7), or AAV-K174Q tau (KQ, n=7) (a) or NI (n=10), AAV-K174Q tau (KQ, n=9), or AAV-K174R tau (KR, n=9) (b). *** $p < 0.001$, * $p < 0.05$, one-way ANOVA, Tukey-Kramer posthoc analyses. Scale bar, 500 μm. (**c, e**) Hippocampal expression of K174Q tau leads to hyperactivity in the open field test or reduced spontaneous alterations in the Y-maze. (c) Mice injected with K174Q tau exhibited higher accumulative total activity than those injected with WT (*left*) or with K174R tau (*right*). (e) Mice injected with K174Q showed significantly lower % alternations in the Y-maze than those injected with WT *(left*) or K174R tau (*right*). n=9 (NI, WT, vs. KQ); n=10 (NI), 8 (KQ), 9 (KR). * $p<0.05$, one-way ANOVA, Dunnett post hoc analyses. (**d**) The extent of hyperactivity in the

open field positively correlated with the levels of tau monomers in mice injected with AAV-K174Q tau (KQ, n=18). Pearson correlation analyses. (**f–i**) Hippocampal expression of K174Q tau impaired spatial learning in MWM. K174Q tau (f), but not K174R tau (h), impaired spatial learning in both the naive and the reversal learning phases. * $p < 0.05$, ** $p < 0.01$, multilevel mixed-effects linear regression model (the naïve and reversal phases were analyzed separately). In probe trials, mice expressing K174Q tau, not WT tau, crossed the new platform location significantly fewer times that NI controls (g). n=9 mice/condition (f,g). n=10 (NI), 9 (KQ), 9 (KR) (h,i). ** $p<0.01$, *** $p<0.001$, two-way ANOVA, Bonferroni post-tests. Values are means ± SEM (a,b. c, e, f–i). WT, wild-type.

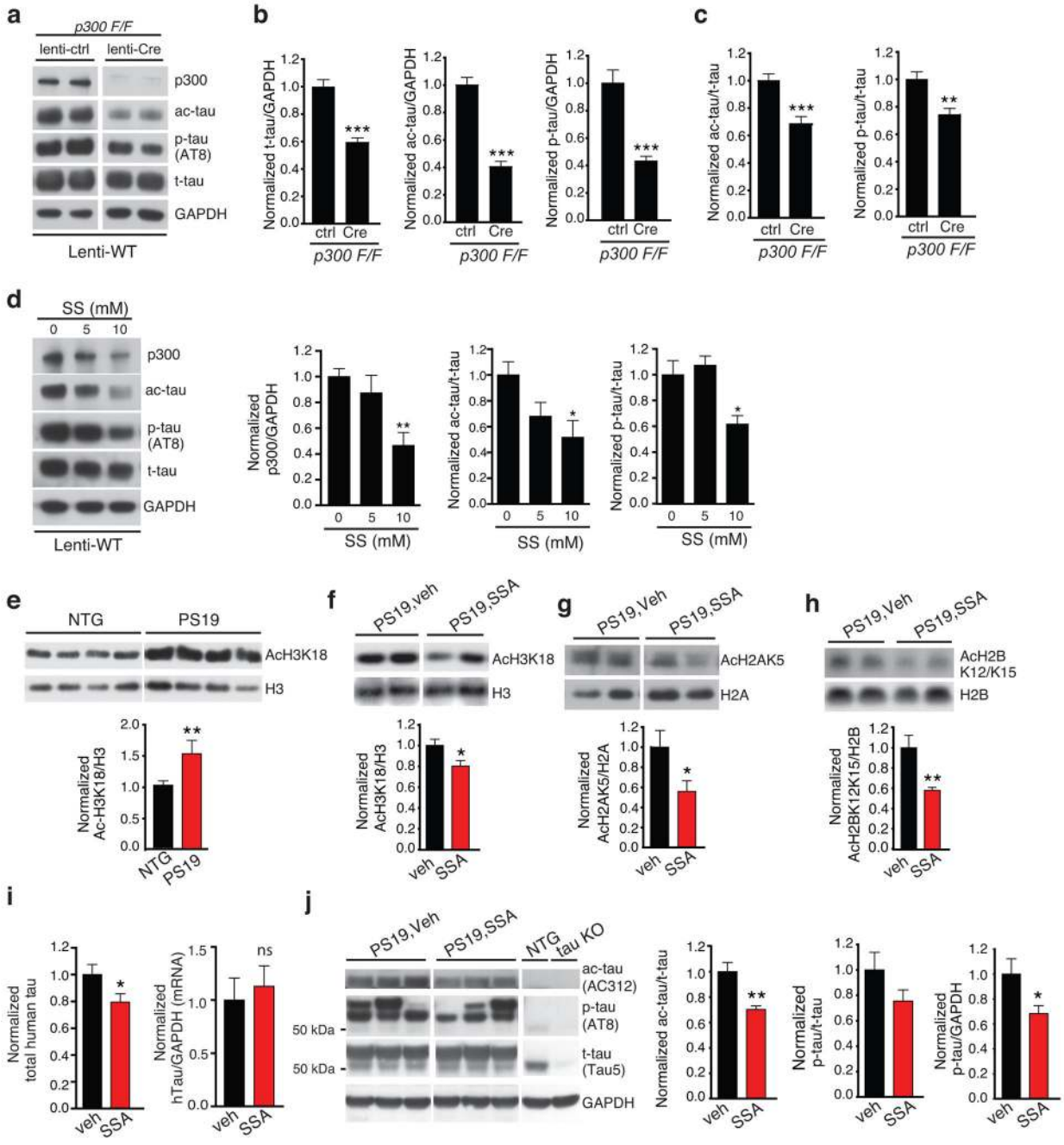

Figure 4. Salicylate Inhibits p300 and Reduces Ac-Tau (K174) In Cultured Neurons and PS19 mice

(**a–c**) Genetic deletion of p300 lowers levels of ac-K174, p-tau and total tau. (a) Lysates from primary mouse neurons that were derived from $p300^{F/F}$ pups, and infected with lenti-WT tau and lenti-control or lenti-cre virus were immunoblotted with anti-p300, ac-tau (AC312), p-tau (AT8), or t-tau (Tau5) antibody. (b) Quantification of levels of total tau (t-tau) (*left*), ac-K174 (*middle*), and AT8-positive p-tau (*right*). (c) Quantification of the levels of ac-K174 (*left*) or p-tau (*right*) relative to t-tau. Levels in non-treated cells were set as 1. n=11 from three independent experiments, *** $p < 0.001$, ** $p < 0.01$, unpaired student t-

test (ac-tau), Kruskal-Wallis test (p-tau). (**d**) Rat primary cortical neurons infected with lenti-WT tau were treatment with 0, 5, 10 mM salicylate for 24 hr (DIV 12). Representative immunoblot of p300, ac-tau, p-tau and t-tau. Quantification of the levels of p300 (*left*), ac-tau (*middle*) or AT8-positive p-tau (*right*) relative to t-tau, in primary rat neurons treated with salicylate. Levels in non-treated cells were set as 1. n = 4 from 4 independent experiments.. *, $p < 0.05$, **, $p < 0.01$, one –way ANOVA, *Tukey-Kramer* post-hoc analyses. (**e**) Representative immunoblot and quantification of ac-H3K18 and H3 in cortical histone extract from 10–11-month-old NTG and PS19 littermates. Levels in NTG group were set as 1. n=9 mice/group, ** $p < 0.01$, unpaired student t-test. (**f–h**) Oral gavage of SSA (225 mg/kg) inhibits p300 activity in the brain. Representative immunoblot and quantification of ac-H3K18 and H3 (f, male, n=11/group), ac-H2AK5 and H2A (g, female, n=8/group) or ac-H2BK12K15 and H2B (h, male, n=11/group). Levels in vehicle-treated group were set as 1. * $p < 0.05$,unpaired student t-test. (**i**) SSA treatment lowers levels of total hTau protein, but not mRNA. Levels of total hTau protein were measured by ELISA (*left*). Levels of hTau mRNA were measured by qRT-pCR (*right*). Levels in vehicle-treated group were set as 1. n=11 mice/condition, 10–11 months old male, * $p < 0.05$, unpaired student t-test. ns=not significant. (**j**) SSA treatment lowers levels of ac-tau relative to total tau. Representative immunoblot of ac-tau (AC312), p-tau (AT8), and t-tau (Tau5). Vehicle-treated non-transgenic NTG and tau KO mice were included as controls. Quantification of ac-tau (*left*) or AT8-positive p-tau relative to t-tau (*middle*) or GAPDH (*right*), in the soluble hippocampal lysates from PS19 mice treated with vehicle or SSA. Levels in vehicle-treated group were set as 1. n=8 mice/condition, 10–11 months old female, ** $p < 0.01$, *, $p < 0.05$, unpaired student t-test. Values are mean ± SEM (b–j). WT, wild-type. NTG, non-transgenic.

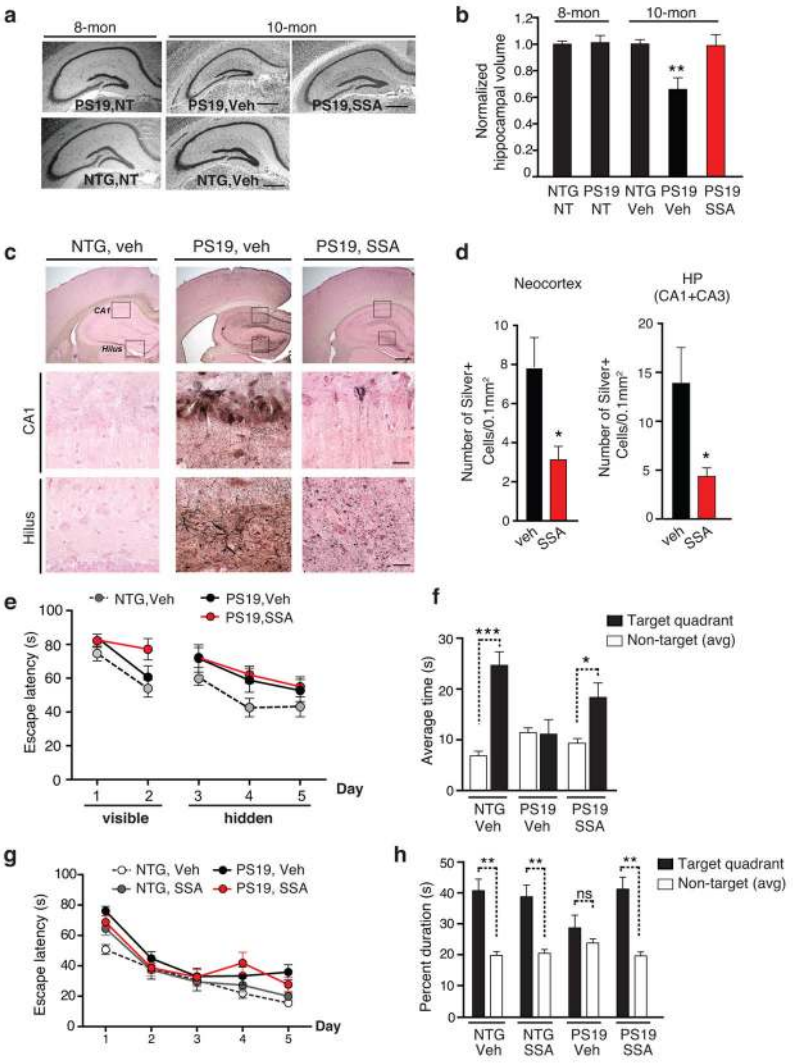

Figure 5. Salsalate Treatment Prevents Hippocampi Atrophy, Reduces Tau Pathology and Rescues Spatial Memory Deficits in PS19 Mice

(**a–b**) SSA treatment prevented hippocampal volume loss. (a) Representative nissl staining of hippocampus from 8-month-old NTG and PS19 mice before the treatment (non-treated, NT), 10 month-old vehicle-treated NTG, vehicle- or SSA-treated PS19 mice. Scale bar, 500 μm. (b) Quantification of hippocampal volume. n=6 (NTG, NT), 9 (PS19, NT), 8 months old. n=9 (female NTG, veh), 6 (female PS19, veh), 6 (female PS19, SSA), 10–11 months old, ** $p < 0.01$, one-way ANOVA, Tukey-Kramer post hoc analyses. (**c–d**) SSA treatment reduced NFTs in PS19 mice. (c) Example of Gallyas staining images of vehicle-treated female NTG mice, and female PS19 mice treated with vehicle or SSA. Scale bar: 250 μm (*upper*); 25 μm (*middle, lower*) (d) Quantification of silver-positive cells or neurites in neocortex and hippocampus (CA1+CA3) of vehicle- or SSA treated PS19 mice. n=8 mice/genotype/treatment, 10–11 months old, * $p < 0.05$, unpaired student t-test. (**e–h**) SSA treatment ameliorated spatial memory loss in fixed-location dry maze and in MWM. (e) No significant difference in learning rate was observed among the groups in fixed location dry maze; Day 1–2, training with visible hole; Day 3–5, learning with hidden hole. (f) NTG or

SSA-treated PS19 mice, but not vehicle-treated PS19 mice, showed preference to the target quadrant. n=10 (female NTG, veh), 8 (female PS19, veh), 8 (female PS19, SSA), 10–11 months old. (g) Learning rate did not differ among the groups in MWM. (h) SSA treatment restored spatial memory deficits in PS19 mice. NTG or SSA-treated PS19 mice, but not vehicle-treated PS19 mice, showed preference to the target quadrant. n=13 (male NTG, veh), 15 (male NTG, SSA), 11 (male PS19, veh), 10 (male PS19, SSA), 9–10 months old. The multilevel mixed-effects linear regression model was used to assess the learning curve (e, g). *** $p < 0.001$, ** $p < 0.01$, * $p < 0.05$, paired student t-test. Values are means ± SEM (b, d, e–h). NTG, non-transgenic.

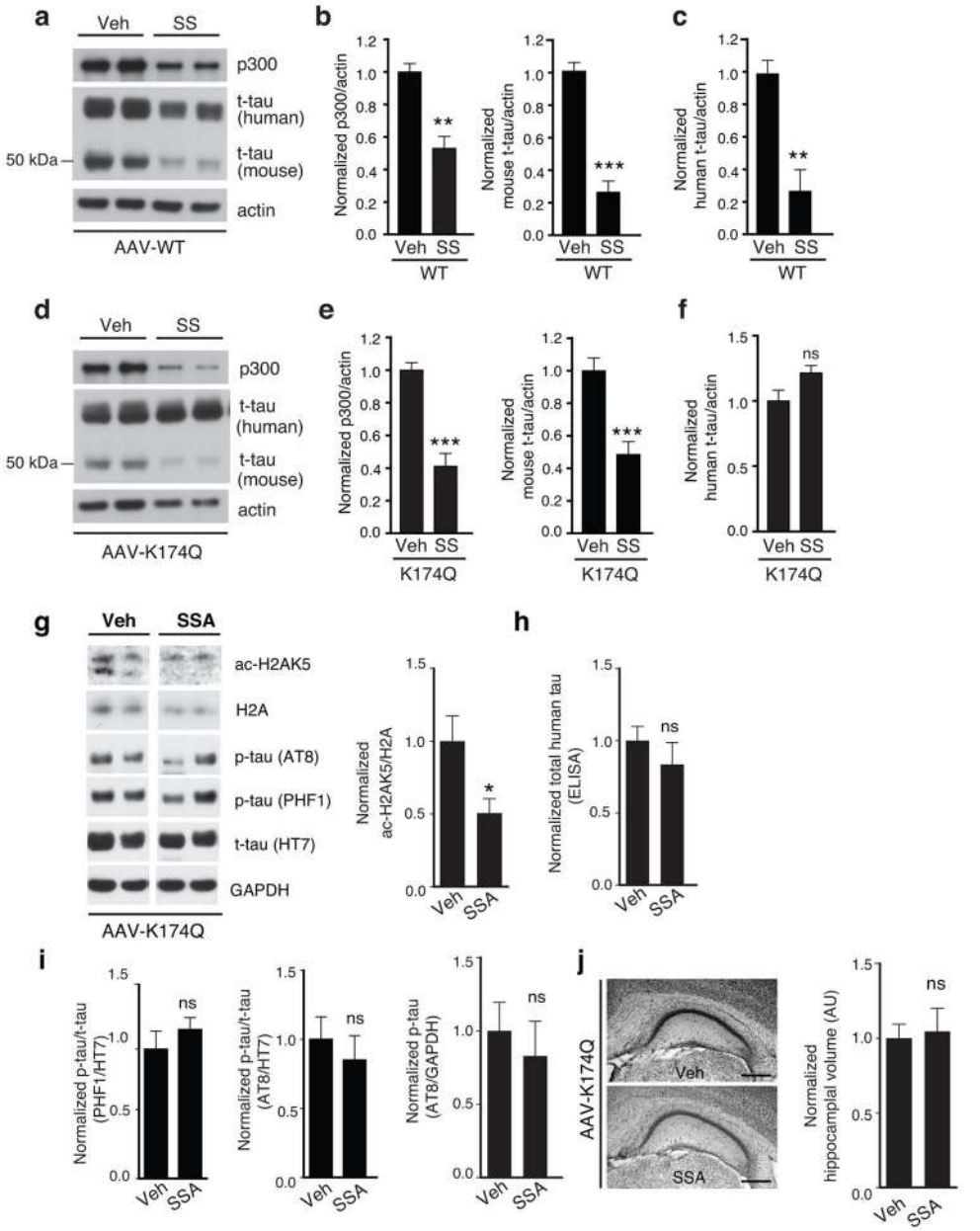

Figure 6. Tau-lowering and Protective Effects of SSA/Salicylate Involve Ac-K174 Inhibition

(**a–f**) SSA treatment lowers levels of WT tau, but not K174Q tau in cultured neurons. Rat primary cortical neurons infected with AAV-WT or AAV-K174Q tau were treated with 5 mM SS for 24 hr (DIV 12). (a, d) Representative immunoblot of p300 and t-tau (human or mouse). Quantification of levels of p300 (b, e; *left*), mouse t-tau (b, e; *right*) and human t-tau (c, f) after SS- or veh-treatment. Levels in veh-treated cells were set as 1. n=4 from two independent experiments. *** $p < 0.001$, ** $p < 0.01$, unpaired student t-test. (**g,h**) SSA treatment failed to lower t-tau in mice expressing K174Q tau. (g, *left*) The representative immunoblot of antibodies against ac-H2AK5 and H2A, AT8, PHF1, HT7 or GAPDH. (g, *right*) Quantification showing that levels of ac-H2AK5/H2A were lower in SSA-treated than veh-treated mice. (h) ELISA assay shows that levels of total K174Q tau were not

significantly affected by SSA treatment. n=11 (vehicle), n=10 (SSA), ns = not significant, unpaired student t-test. (**i**) Levels of PHF1-positive p-tau normalized to HT7 (*left*), or levels of or AT8-positive p-tau normalized to HT7 (*middle*) or GAPDH (*right*) were not affected by SSA treatment. n=11 (vehicle), n=10 (SSA), * $p<0.05$, ns = not significant, unpaired student t-test. (**j**) SSA treatment failed to protect against atrophy mice expressing K174Q tau. (*left*) The representative nissl-stained images of hippocampus treated with either vehicle or SSA. Scale bar: 500 μm. (*right*) Quantification of hippocampal volume showing no significant difference. n=11 (vehicle), n=10 (SSA), ns = not significant, unpaired student t-test. Values are means ± SEM (b, c, e, f, h–j). WT, wild-type.